Elastic, vibrational, and thermodynamic properties of $Sr_{10}(PO_4)_6F_2$ and $Ca_{10}(PO_4)_6F_2$ from first principles*

Xianggang Kong(孔祥刚)[1], Zhihong Yuan(袁志红)[1], You Yu(虞游)[2], Tao Gao(高涛)[1,3,†], and Shenggui Ma(马生贵)[1]

[1] *Institute of Atomic and Molecular Physics, Sichuan University, Chengdu* 610065, *China*
[2] *College of Optoelectronic Technology, Chengdu University of Information Technology, Chengdu* 610225, *China*
[3] *Key Laboratory of High Energy Density Physics and Technology of Ministry of Education, Sichuan University, Chengdu* 610064, *China*

(Received 13 April 2017; revised manuscript received 15 May 2017; published online 20 June 2017)

The electronic, elastic, vibrational, and thermodynamic properties of $Sr_{10}(PO_4)_6F_2$(Sr-FAP) and $Ca_{10}(PO_4)_6F_2$(Ca-FAP) are systematically investigated by the first-principles calculations. The calculated electronic band structure indicates that the Sr-FAP and Ca-FAP are insulator materials with the indirect band gap of 5.273 eV and 5.592 eV, respectively. The elastic constants are obtained by the "stress–strain" method, and elastic modulus are further evaluated and discussed. The vibrational properties, including the phonon dispersion curves, the phonon density of states, the Born effective charge, and associated longitudinal optical and transverse optical (LO–TO) splitting of optical modes, as well as the phonon frequencies at zone-center are obtained within the linear-response approach. Substitution of Ca by Sr causes phonon frequencies to shift to lower values as expected due to the mass effect. Additionally, some phonon-related thermodynamic properties, such as Helmholtz free energy F, internal energy E, entropy S, and specific heat C_V of Sr-FAP and Ca-FAP are predicted with the harmonic approximation. The present calculated results of two apatites are consistent with the reported experimental and theoretical results.

Keywords: Sr-FAP, Ca-FAP, TDOS, elastic modulus, thermodynamic properties

PACS: 63.20.dk, 65.40.Ba, 71.20.–b, 65.40.gd **DOI:** 10.1088/1674-1056/26/8/086301

1. Introduction

Calcium fluorapatite ($Ca_{10}(PO_4)_6F_2$) is the most common mineral apatite, which has attracted extensive attention due to its well-known industrial and biological applications. Numerous experimental and theoretical studies have been carried out on this compound.[1–14] Moreover, Ca-FAP as a suitable host for various substituents has attracted more and more researchers on the substitution of Ca-FAP.[15–18] Strontium (Sr) is one of the most common substituents in fluorapatite. The Sr fluorapatite is of considerable significance in biology, geology, and materials science.[18–21] Since the ionic radius of Sr (1.13 Å) is larger than that of the Ca (0.99 Å), with the incorporation of Sr in fluorapatite crystal, the distance of Sr–F will be larger than that of Ca–F and then may lead to the modifications in lattice parameters and some physical properties. In this paper, the Sr-richest fluorapatite Sr-FAP will be discussed. Sr-FAP was firstly found by the central research laboratory of the General Electronic Company Limited in 1964[22] and accepted as a new species by the IMA CNMNC in 2008, then was named as stronadelphite in 2010.[23]

The interest in the crystal Sr-FAP is defined by some of its practical applications. Firstly, Sr-FAP is a well-known host for functional rare earth ions with subsequent applications as fluorescent and laser materials.[24–31] Secondly, the Sr in Sr-FAP will used as a petrogenetic indicator in geology.[18] Thirdly, owing to the biological function of Sr and F,[15] Sr-FAP has been viewed as a promising material in medical fields, for instance drug delivery, disease diagnosis, and therapy.[31] There are some investigations that have been carried out on the crystal Sr-FAP. The crystal structure of Sr-FAP was determined by Swafford[32] with x-ray diffraction (XRD) in 2002. Several groups have studied the Infrared and Raman spectra of crystal Sr-FAP. Schulte[33] and Carl Bonner[34] have reported the Raman scattering of crystal Sr-FAP at ambient condition, while Shuangmeng Zhai[35] carried out the investigation of the Raman scattering under high pressure conditions. The IR spectroscopy of Sr-FAP was studied by Aissa.[36] The thermal expansion of Sr-FAP was studied by high temperature x-ray diffraction and differential thermal analysis.[37] Recently, Baoyan Chai researched the precipitation and growth mechanism of diverse Sr-FAP particles.[31] Theoretically, the electronic structure of Sr-FAP was given in the Materials Project.[38] The elastic properties of pure crystal are predicted by Rabone using the program GULP[39] and the Sr-doped fluorapatite is calculated by Goryaeva within the semi-empirical approach.[40] The dynamical stability of Sr-FAP is confirmed

*Project supported by the National High Technology Research and Development Program of China (Grant No. 2015AA034202) and the National Natural Science Foundation of China (Grant No. 11305147).
†Corresponding author. E-mail: gaotao@scu.edu.cn
© 2017 Chinese Physical Society and IOP Publishing Ltd

with the density functional theory by Balachandran.[41] However, no vibrational, and thermodynamics property has been reported. In this paper, we aim at providing the investigation of the electronic, elastic, vibrational, and thermodynamic properties of the crystal Sr-FAP from the theoretical insight. Taking into account that Sr-FAP is isomorphous with Ca-FAP, a systematic investigation on Ca-FAP has also been given in our work for the reason of comparison. All the calculations are carried out using first-principles calculations implemented in the Vienna *Ab-initio* Simulation Package (VASP).[42–44]

The remainder of this paper is structured as follows. In Section 2, the computational method is briefly described. Section 3 is devoted to the results and discussions of the electronic, elastic, vibrational and thermodynamic properties of Sr-FAP and Ca-FAP and the comparison with other available experimental and theoretical data. Finally, the summarized conclusions are given in Section 4.

2. Computational details

All the calculations are carried out using a first-principles calculation implemented in the VASP.[42] The Generalized Gradient Approximation (GGA)[45] with Perdew–Wang (PW91) function is applied to describe the Coulomb interactions between ions and electrons, and the valence electron configurations Sr $4s^2 4p^6 5s^2$, Ca $3p^6 4s^2 d^{0.01}$, P $3s^2 3p^3$, O $2s^2 2p^4$, F $2s^2 2p^5$ are chosen for these elements, respectively. The primitive cells $M_{10}(PO_4)_6X_2$ (M = Ca, Sr), which contain 42 atoms, are chosen in our calculations in order to reduce the computational cost. The energy cutoff of 700 eV is chosen to determine the number of plane waves in expansion and the k-point mesh is set at $2\pi \times 0.04$ Å^{-1} for sampling in the irreducible Brillouin zone (BZ)[46] during our calculations. For the sufficient precision in our calculations, both the kinetic-energy cutoff and k-point sampling have been carefully tested. By minimizing the total energy, we obtain the fully relaxed equilibrium structure. The optimization is stopped when the calculated forces are converged to be less than 0.01 eV/Å and the total energy is converged to be less than 10^{-7} eV.

After structural optimization, the elastic constants at the equilibrium structures are calculated using the stress–strain method which has been applied to a large number of complex ceramic crystals.[44] From elastic constants C_{ij}, the elastic modulus is further evaluated using the Voigt–Reuss–Hill approximation. The dynamical properties including phonon dispersion curves and phonon density of states, phonon frequencies at zone-center as well as the Born effective charge and LO–TO splitting of optical modes are obtained by the linear response approach[47–49] as implemented in the VASP code combined with the PHONOPY code.[50] Furthermore, some phonon-related thermodynamic properties such as Helmholtz free energy F, internal energy E, entropy S, and specific heat constant volume C_V are predicted within the harmonic approximation.

3. Results and discussions

3.1. Structure optimization and electronic properties

The hexagonal crystal structure Sr-FAP and Ca-FAP belong to the space group $P6_3/m$ (C_{6h}^2) and contain one molecule per primitive cell. The structure is given for reference in Fig. 1, which is exported by the VESTA code.[51] It can be seen that the crystal structure consists of six PO_4 tetrahedrons surrounded by ten Sr atoms and two F atoms located in columns parallel to the six-fold helix axis. The ten Sr atoms occupy two non-equivalent crystallographic symmetry sites, Sr1 at 4f and Sr2 at 6h. The six PO_4 groups also occupy Wyckoff position 6h, in expanded triangular positions, while the oxygen atoms are arranged in three unique environments. The two F atoms that occupy the 2a position, namely the center of Sr triangles on mirror planes at $z = 0.25$ and $z = 0.75$.

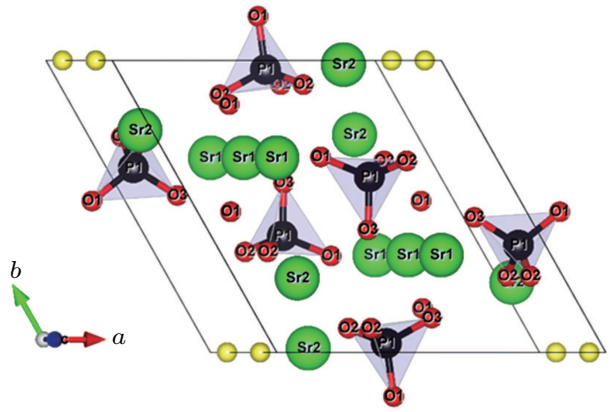


Fig. 1. (color online) The crystal structure of Sr-FAP with atoms labeled on the basis of element and symmetrical characteristic. (The figure is exported by the VESTA code[51]).

The calculated crystal structure parameters of Sr-FAP and Ca-FAP are summarized in Table 1 along with the experimental and other theoretical values. The lattice parameters in Table 1 are in close agreement with the experimental values within a difference of 1%–2%, which is due to the fact that GGA tends to overestimate the structure parameters. Therefore, the optimized results pave the way for a further study of various properties of two apatites. And from Table 1, we note that the bond length increased with the replacement of Ca by Sr, and the lattice parameters and cell volume of Sr-FAP are larger than those of Ca-FAP, which can be explained by the fact that the ionic radius of Sr is larger than that of the Ca. The modifications of structural constants may result in the change of some physical properties for two apatites.

Table 1. Optimized and experimental structure parameters of Sr-FAP and Ca-FAP.

Apatite	Lattice parameters/Å		V/Å^3	c/a	Refs.
	a	c			
Sr-FAP	9.831	7.343	614.73	0.747	this work
	9.678	7.275	590.1	0.752	expt.[a]
	9.841	7.365	617.80	0.748	other cal. [b]
Ca-FAP	9.467	6.896	535.22	0.728	this work
	9.364	6.881	522.55	0.734	expt.[c]
	9.489	6.928	540.26	0.730	other cal.[d]
	Bond length/Å				
Sr_2-F	2.434	Ca_2-F	2.319		this work
Sr_2-F	2.393[a]	Ca_2-F	2.311[c]		expt.[a,c]

[a] Ref. [32]; [b]Ref. [38]; [c]Ref. [6]; [d]Ref. [38]

The calculated band structure of Sr-FAP and Ca-FAP are displayed in Fig. 2. Obviously, two apatites are insulator materials and there is a difference only in the width of band gap. For two apatites, the bottom of the conduction band (CB) is situated at the Γ point and the top of the valence band (VB) is localized between the Γ point and the M point, which reveals that both of them are characterized with the indirect band gaps. The calculated band gaps together with other theoretical values for two apatites are listed in Table 2. Our calculated results are in good agreement with the other theoretical results and the band gap of Sr-FAP is smaller than that of Ca-FAP. Another important point to notice is that the density functional theory (DFT) predictions always underestimate the true band gap, so the real values may be somewhat higher than calculated ones here.

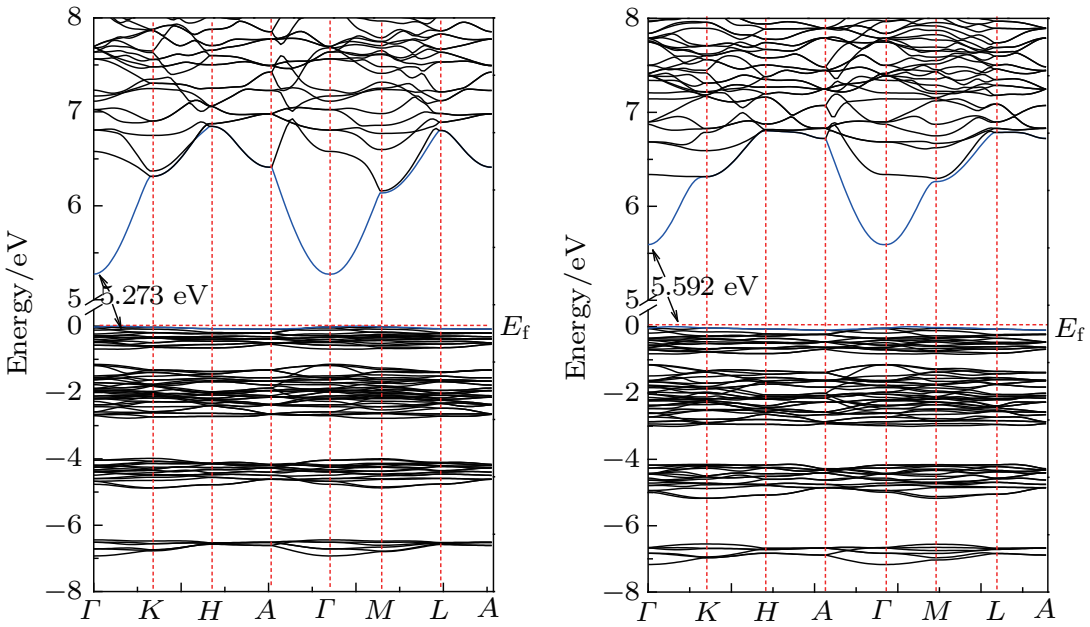


Fig. 2. (color online) Calculated band structures for Sr-FAP (left) and Ca-FAP (right). The Fermi level (E_f) is aligned to the zero and expressed by a dash line.

Table 2. Calculated band gaps E_g (in unit eV) of Sr-FAP and Ca-FAP.

Apatite	This work	Other cal.[a]	Other cal.[b,c]
Sr-FAP	5.273	5.212	5.35[b]
Ca-FAP	5.592	5.515	5.47[c]

[a] Ref. [38];[b] Ref. [41]; [c]Ref. [13]

The total density of states (TDOS) together with the partial densities of states (PDOS) of the PO_4 group, Sr (or Ca) and F atoms for two apatites are shown in Fig. 3. The DOSs of two apatites look very similar to each other. The DOSs below Fermi energy in the energy range of -10 eV to 0 eV are described by four main peaks (A–D). Peak A mostly derived from O 2p and P 3s states with some O 2s contribution, while peak B is dominated by O 2p and P 3p states. As for peaks C and D, they are mainly composed of the O 2p state with some contribution from the F p state, especially peak C has received approximately 13% of its value from the F p state. The conduction band is chiefly contributed from Sr 4d (Ca 3d) states with some mixing of O 2s, O 2p and F p states. There are also four main peaks below -13 eV for Sr-FAP and Ca-FAP. We note that, for two apatites, the peak labeled 1 is primarily from F s states while the peaks labeled 2 and 3 are mainly from the O 2s state and P 3p state with a tiny P 3s state. However, the significant peak labeled 4 is different for two apatites. For Sr-FAP, peak 4 located about -15 eV and contributed from the Sr 4p state with minor contribution of the O 2s state, while for Ca-FAP, peak 4 located about -19.5 eV and contributed from the Ca 3p state with minor contribution of the O 2s state. Additionally, we also find that Ca-FAP has a small double peak at -20.5 eV and -17.5 eV from its Ca 3p state, and Sr-FAP has a small single peak at -17 eV from its Sr 4p state.

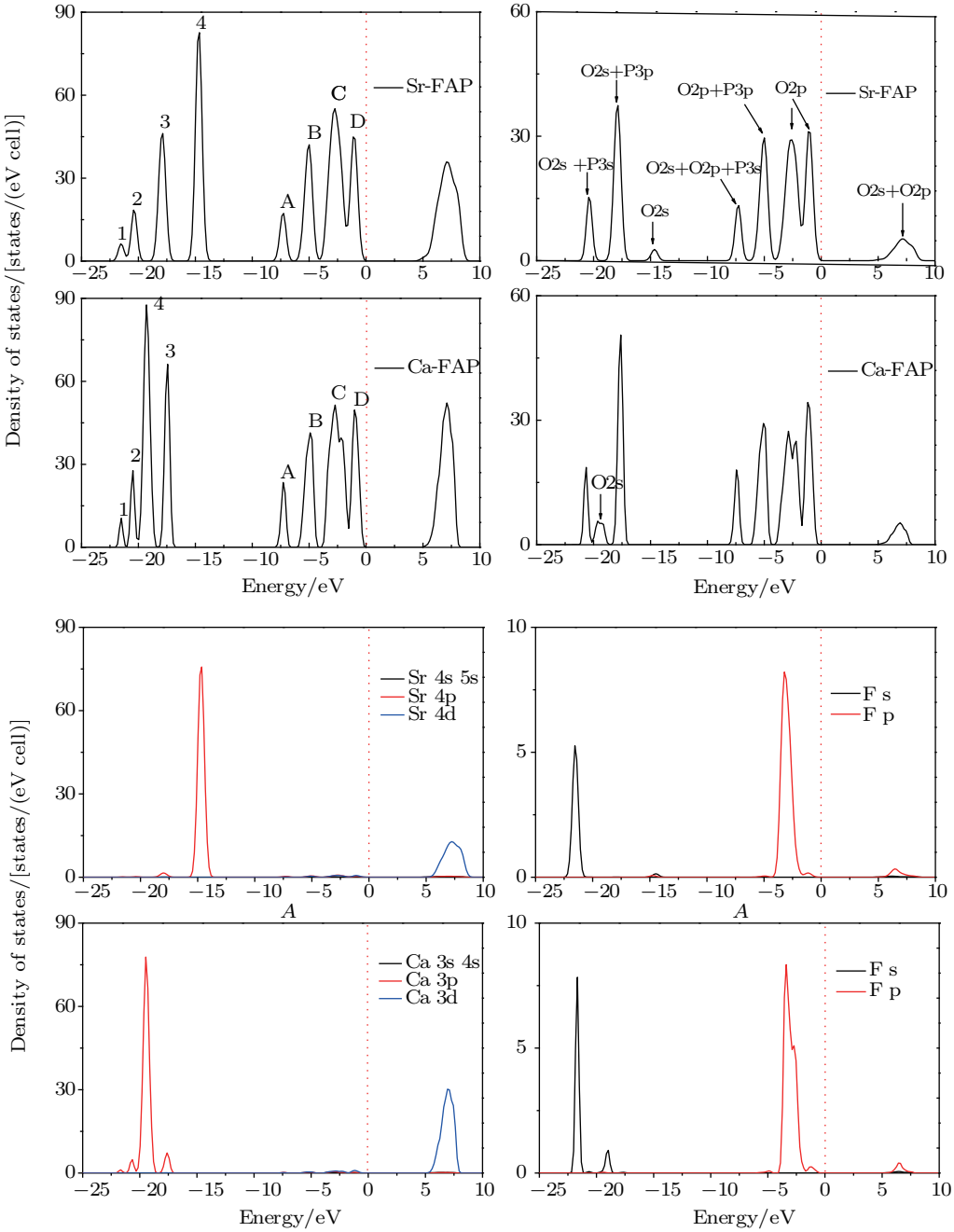


Fig. 3. (color online) Total density of states (TDOS) and partial density of states (PDOS) of Sr-FAP and Ca-FAP.

3.2. Elastic properties

Elastic constants are very important mechanical parameters of materials, which provide useful information about the stability and mechanical properties. In the present work, the "stress-strain" method is used to obtain the elastic constants of Sr-FAP and Ca-FAP, which is based on the well-known relationship $\sigma_i = \sum_{j=1}^{6} C_{ij}\varepsilon_j$. The C_{ij} is the elastic constant of the relaxed material, which are determined by analyzing the small stress σ_i caused by forcing a small strain ε_j ($j = 1, \ldots, 6$) to the optimized unit cell.[44] For a hexagonal structure, the matrix of C_{ij} has the form:[52]

$$\begin{pmatrix} C_{11} & C_{12} & C_{13} & 0 & 0 & 0 \\ C_{12} & C_{11} & C_{13} & 0 & 0 & 0 \\ C_{13} & C_{13} & C_{33} & 0 & 0 & 0 \\ 0 & 0 & 0 & C_{44} & 0 & 0 \\ 0 & 0 & 0 & 0 & C_{44} & 0 \\ 0 & 0 & 0 & 0 & 0 & (C_{11}-C_{12})/2 \end{pmatrix}.$$

Five independent components C_{11}, C_{12}, C_{13}, C_{33}, C_{44} of Sr-FAP and Ca-FAP are obtained and presented in Table 3. It is found that they are in good agreement with the experimental and other theoretical data.

The mechanical stabilities of the two apatites could be discussed based on elastic constants. For a hexagonal structure the mechanical stability criteria are: $C_{11} > 0$, $C_{44} > 0$,

$C_{11} > C_{12}$, $(C_{11}+C_{12})\,C_{33} - 2C_{13}^2 > 0$.[53] Obviously, the calculated elastic constants in Table 3 satisfy all the above criteria, indicating that Sr-FAP and Ca-FAP in hexagonal structure are mechanically stable. From Table 3, we find that, for the two apatites, the calculated value of C_{33} is higher than that of C_{11}, which means that the a axis is more compressible than the c axis for Sr-FAP and Ca-FAP.[52]

From the calculated elastic constants, the elastic modulus such as the bulk modulus B, shear modulus G, Young modulus E, and Poisson's ratio ν are evaluated according to the Vioght–Reuss–Hill approach[54] by the following equations:

$$B_{\mathrm{V}} = \frac{1}{9}\left(2C_{11}+C_{33}+2C_{12}+4C_{13}\right), \tag{1}$$

$$B_{\mathrm{R}} = \frac{(C_{11}+C_{12})C_{33}-2C_{13}^2}{C_{11}+C_{12}+2C_{33}-4C_{13}}, \tag{2}$$

$$B_{\mathrm{H}} = \frac{1}{2}\left(B_{\mathrm{R}}+B_{\mathrm{V}}\right), \tag{3}$$

$$G_{\mathrm{V}} = \frac{1}{30}\left(7C_{11}+12C_{44}+2C_{33}-5C_{12}-4C_{13}\right), \tag{4}$$

$$G_{\mathrm{R}} = \frac{5\left\{\left[(C_{11}+C_{12})C_{33}-2C_{13}^2\right]C_{44}C_{66}\right\}}{2\left\{3B_{\mathrm{V}}C_{44}C_{66}+\left[(C_{11}+C_{12})C_{33}-2C_{13}^2\right](C_{44}+C_{66})\right\}},$$

$$G_{\mathrm{H}} = \frac{1}{2}\left(G_{\mathrm{R}}+G_{\mathrm{V}}\right), \tag{5}$$

$$E_{\mathrm{H}} = \frac{9B_{\mathrm{H}}G_{\mathrm{H}}}{3B_{\mathrm{H}}+G_{\mathrm{H}}}, \tag{6}$$

$$\nu_{\mathrm{H}} = \frac{3B_{\mathrm{H}}-2G_{\mathrm{H}}}{2\left(3B_{\mathrm{H}}+G_{\mathrm{H}}\right)}. \tag{7}$$

Table 3. Calculated and experimental elastic constants (GPa) for Sr-FAP and Ca-FAP.

Apatite	C_{11}	C_{12}	C_{13}	C_{33}	C_{44}	Refs.
Sr-FAP	127.1	46.4	47.8	147.4	37.1	this work
	125.8	44.8	47.0	143.2	36.1	other cal.[a]
	137.9	64.4	49.7	145	42.3	other cal.[b]
	142	63	47	146	40	other cal.[c]
Ca-FAP	134.6	37.4	64.7	174.2	37.3	this work
	126.4	35.8	63	167.8	35	other cal.[d]
	143.4	44.5	57.5	180.5	41.5	expt.[e]

[a]Ref. [38]; [b]Ref. [39]; [c]Ref. [40]; [d]Ref. [12]; [e]Ref. [53]

The results of elastic modulus are listed in Table 4. Bulk modulus B is a measurement of materials resistance to volume change and shear modulus G reflecting their resistance to shape change, thus a high (less) B/G ratio reflects a tendency for ductility (brittleness). The critical value of B/G is evaluated to be 1.75 according to the Pugh criterion.[52,55] Our calculated results suggest that Sr-FAP and Ca-FAP are ductile, and Sr-FAP has the more brittleness. Young's modulus E is defined as the ratio of line stress and liner strain, which gives information about the measure of the stiffness of the solid. The larger the Young modulus, the stiffer the material.[49] In the present work, the Young modulus E of Sr-FAP is smaller than that of Ca-FAP, so the Ca-FAP is stiffer than Sr-FAP. The Poisson ratio υ can be interpreted as a measure of bonding nature, and the typical value of Poisson's ratio for an ionic material is 0.25,[56] whereas for a covalent material it is small to 0.1. In our case the Poisson ratios for two apatites are larger than 0.25, which implies the ionic bonding is predominant in the Sr-FAP and Ca-FAP.

Table 4. Calculated and experimental bulk modulus B, shear modulus G, Young's modulus E, Poisson's ratio υ of Sr-FAP and Ca-FAP.

	Sr-FAP			Ca-FAP		
	Present	Other cal.[a]	Other cal.[b]	Present	Other cal.[c]	Expt.[d]
B_{V}/GPa	76.1	74.7		86.3		
B_{R}/GPa	75.8	74.4		82.6		
B_{H}/GPa	76.0	74.5	82	84.4	81	86.5
G_{V}/GPa	40.2	39.3		43.1		
G_{R}/GPa	39.9	39.0		42.1		
G_{H}/GPa	40.1	39.1	41	42.6	39.8	46.7
$B_{\mathrm{H}}/G_{\mathrm{H}}$/GPa	1.89			1.98		
E_{H}/GPa	102.3			109.4		
υ/GPa	0.28	0.28		0.29		

[a]Ref. [38]; [b]Ref. [40]; [c]Ref. [12]; [d]Ref. [53]

3.3. Vibrational properties

3.3.1. Phonon dispersion curves and density of states

The vibrational spectrum is essential to understand the nature of a material, and many physical properties of materials depend on their vibrational properties. After structural relaxation, the vibrational properties are investigated by the density functional perturbation theory (DFPT). The calculated phonon dispersion curves (including the LO–TO splitting for infrared active modes) of Sr-FAP and Ca-FAP are plotted in Fig. 4. It is well known that phonon dispersion curves can indicate the stability of the crystal. Obviously, no imaginary phonon frequency has been shown in Fig. 4, which suggests the optimized Sr-FAP and Ca-FAP are dynamically stable. As shown in Fig. 4 that the phonon behaviors are generally similar for two apatites, but the Ca-FAP has higher phonon frequencies than Sr-FAP since atomic mass of Ca atom is slighter than that of Sr atom. Since the primitive cell of hexagonal Sr-FAP and Ca-FAP contain 42 atoms, the complete phonon spectrum consists of 126 dispersion curves, namely 3 acoustical modes and 123 optical modes. The standard group-theoretical analysis based on the $P6_3/m$ space group predicts that the Sr-FAP and Ca-FAP structures share the same optical phonon modes at the Γ point, as shown in the following irreducible representations:

$$\Gamma_{\mathrm{opt}} = 12A_{\mathrm{g}}+8E_{1\mathrm{g}}+13E_{2\mathrm{g}}+8A_{\mathrm{u}}+12E_{1\mathrm{u}}+12B_{\mathrm{u}}+9B_{\mathrm{g}}+8E_{2\mathrm{u}},$$

Of these modes, A_{g}, $E_{1\mathrm{g}}$, and $E_{2\mathrm{g}}$ are corresponding to Raman-active modes, whereas the A_{u} and $E_{1\mathrm{u}}$ are IR modes, B_{u} and $E_{2\mathrm{u}}$ are silent modes, and the A and E modes are singly and doubly degenerate modes, respectively.

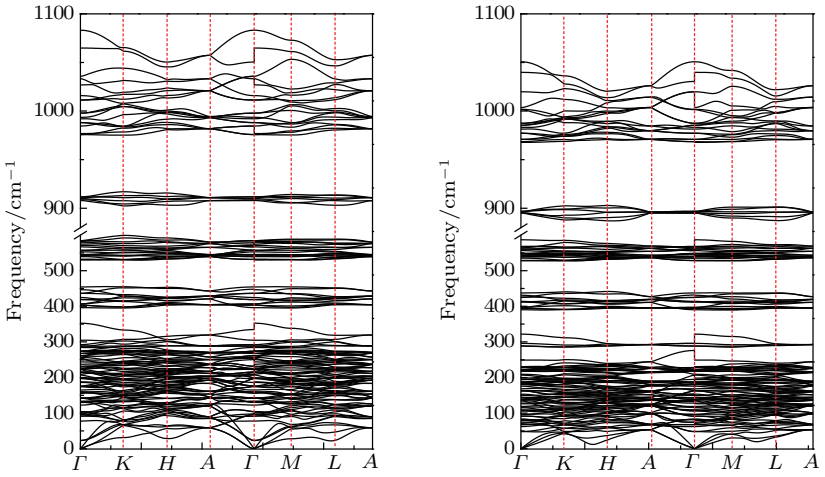


Fig. 4. (color online) Calculated phonon dispersion curves (including LO–TO splitting) for Sr-FAP (left) and Ca-FAP (right).

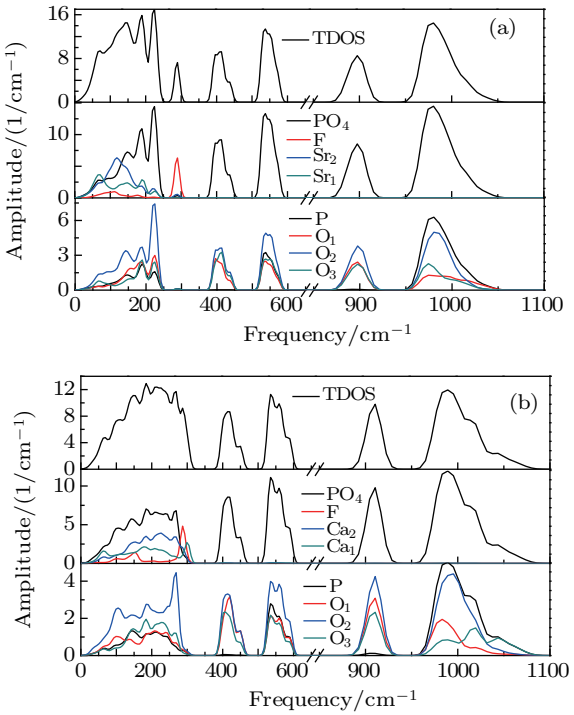


Fig. 5. (color online) Phonon total density of states and phonon partial density of states for Sr-FAP and Ca-FAP.

The phonon total density of states including the phonon partial density of states of the PO_4 group, Sr (Ca) and F atoms are illustrated in Fig. 5. The phonon DOS shapes of two apatites are quite similar. Obviously, the modes range from 350 cm^{-1} to 1100 cm^{-1} are contributed from the vibrations of PO_4 groups for the two apatites. For all of these modes, the first band corresponds to the stretching vibrations for the O–O bond. The second band mainly comes from bending vibrations for the O–O bond along with the P–O bond. The rest of the high frequencies mostly correspond to symmetric stretching vibration of the O–O bond and asymmetric stretching vibration of the P–O bond, respectively. The massive modes below 300 cm^{-1} involving the vibrations of all bonds majorly devote to thermodynamics. Due to the fact that the Sr atom is heavier than that of the Ca atom, Sr-FAP has more low frequencies than Ca-FAP, indicating the increasing trend of the vibrational contribution to thermodynamics.

3.3.2. LO–TO splitting

It is generally known that LO–TO splitting can be considered into the dynamical matrix by a non-analytical contribution, which depends on the Born effective charge (BEC) tensor and the dielectric constant.[46,48] In the present work, BEC tensor (Z^*) and macroscopic static dielectric constant tensor (ε) of two apatites are calculated through the DFPT. The calculated diagonal elements of ε and Z^* of 7 non-equivalent atoms are given in Table 5 and Table 6, respectively. The Z^* for the other atoms of the unit cell can still be obtained by performing the symmetry operations. Because of the hexagonal symmetry of the crystals, three diagonal elements ε_{xx}, ε_{yy}, ε_{zz} of each atom possess two independent components, and Z^*_{xx}, Z^*_{yy}, and Z^*_{zz} own the similar condition. It is noted that the Z^* diagonal components are close to the nominal ionic values of Ca (+2), Sr (+2), O (−2), P (+3), and F (−1) and the Z^* diagonal components of Sr and F in Sr-FAP are somewhat larger than Ca and F

Table 5. Diagonal component of macroscopic static dielectric tensors ε of Sr-FAP and.

Apatite	ε_{xx}	ε_{yy}	ε_{zz}
Sr-FAP	2.807	2.807	2.785
Ca-FAP	2.889	2.889	2.894

Table 6. Diagonal component of Born effective charge tensors Z^* of Sr-FAP and Ca-FAP.

Site	Atom	Z^*_{xx}	Z^*_{yy}	Z^*_{zz}	Atom	Z^*_{xx}	Z^*_{yy}	Z^*_{zz}
4*f*	Sr_1	2.43	2.43	2.61	Ca_1	2.40	2.40	2.57
6*h*	Sr_2	2.56	2.56	2.49	Ca_2	2.49	2.49	2.50
6*h*	P	3.23	3.23	3.03	P	3.27	3.27	3.10
6*h*	O_1	–1.99	–1.99	–1.39	O_1	–1.96	–1.96	–1.44
12i	O_2	–1.48	–1.48	–2.16	O_2	–1.48	–1.48	–2.15
6*h*	O_3	–1.92	–1.92	–1.30	O_3	–1.92	–1.92	–1.32
2*a*	F	–1.59	–1.59	–0.73	F	–1.56	–1.56	–0.75

in Ca-FAP, which means a stronger covalent characteristic for the Sr-F bond from a chemical point of view.

After considering the calculated macroscopic static dielectric tensor and the Born effective charge, the long-range coulomb (dipole-dipole) interaction induces to the splitting of optical modes at the Γ point due to the breaking of degeneracy of the TO and LO phonons at gamma. It can be seen that the splitting of the LO optical and TO optical modes at the Γ point is evident from the phonon dispersion curves that are displayed in Fig. 4. It should be noted that the LO–TO splitting depends upon the direction in which one approaches the gamma point, and this anisotropy is accessible to experiment with. The LO–TO splitting occurs at some IR vibrations and the LO frequency is larger than the TO frequency. Table 7 and Table 8 tabulate the calculated phonon frequencies of Raman and Infrared (including LO–TO splitting) phonon modes as well as the experimental and other theoretical values. Our calculated frequencies are about 8% lower than the experimental values, which is a general feature of DFT calculations that GGA underestimates the phonon frequencies. And our calculated transverse optical (TO) frequencies of Ca-FAP are in good agreement with the results that were reported by Etienne Balan, *et al*. Further analysis, most of the vibrational frequencies in Raman and IR spectra shift to lower frequencies with replacement of the Ca atoms by Sr atoms, which is caused by the larger bond length in Sr-FAP than that in Ca-FAP. Additionally, for two apatites the modes A_u (2), A_u (6), E_{1u} (7), and E_{1u} (10) display very small LO–TO splitting (< 2 cm^{-1}) in our calculations. But the splitting is too small to be observed in the experimental measurement, which suggests that they are barely affected by the long-range Coulomb interaction.

Table 7. The calculated and experimental Raman-active (R) modes at the Γ point of Sr-FAP and Ca-FAP. (unit: cm^{-1}).

	Sr-FAP		Ca-FAP	
Modes	This work	Expt.[a]	This work	Expt.[b]
E_{2g}	67.8		96.6	100
	96.4		133.0	139
	134.7		159.3	177
	163.3		198.8	214
	180.9		223.9	237
	218.1		261.4	277
	288.4		288.3	311
	412.3	442	418.9	445
	539.1	572	544.0	581
	568.1	601	584.5	617
	896.8	951	911.7	965
	970.9	1028	975.8	1033
	987.4	1037	1011.3	1058
E_{1g}	48.2		23.1	44
	91.5		130.1	135
	137.3		175.6	183
	180.3		215.4	233
	227.9		273.3	284
	394.8	421	403.5	431
	548.5	580	557.3	591
	977.2	1027	988.1	1040
A_g	109.3		142.0	160
	139.2		158.7	–
	168.3		209.0	212
	175.7		223.2	231
	194.5		256.8	266
	221.3		284.3	306
	414.0	444	424.8	452
	546.3	580	553.1	591
	561.1	592	574.7	607
	895.3	951	908.7	963
	983.3	1041	993.6	1051
	1001.5	1054	1033.2	1080

[a] Ref. [36]; [b]Ref. [5]

Table 8. The calculated and experimental infrared-active (IR) and LO–TO splitting at the Γ point of Sr-FAP and Ca-FAP. (unit: cm^{-1}).

	Sr-FAP			Ca-FAP				
Modes	This work		Expt.[a]	This work		Expt.[b]	Other cal.[c]	
	LO	TO		LO	TO	LO	TO	TO
A_u (1)	81.1	71.4		97.7	91.9	108	96	90
A_u (2)	115.6	114.8		142.7	142.5			142
A_u (3)	133.6	127.1		175.6	174.2	193	184	173
A_u (4)	224.0	193.5		270.6	243.8		277	238
A_u (5)	278.7	230.5		342.8	273.6	342	304	268
A_u (6)	431.4	430.8	458	448.3	446.7		470	436
A_u (7)	561.3	527.9	582	562.4	530.1	624	582	523
A_u (8)	1034.1	966.9	1026	1063.1	976.8	1120	1030	991
E_{1u} (1)	80.6	74.4		101.1	91.5	115	100	89
E_{1u} (2)	144.3	142.7		188.0	174.8	204	193	166
E_{1u} (3)	183.4	153.2		229.4	206.9		224	203
E_{1u} (4)	198.0	185.6		237.8	231.7	255	243	227
E_{1u} (5)	252.5	221.9		274.2	254.3	296	273	250
E_{1u} (6)	324.0	295.8		362.4	292.3	386	327	286
E_{1u} (7)	425.0	424.9		446.7	446.4		460	437
E_{1u} (8)	539.1	535.3	561	543.1	539.7	588	580	537
E_{1u} (9)	571.0	556.6	594	585.1	567.0	624	604	564
E_{1u} (10)	896.0	895.2	951	910.6	910.0		962	914
E_{1u}(11)	1010.1	968.5	1069	1028.2	984.6	1072	1034	989
E_{1u} (12)	1053.4	1019.8	1080	1075.8	1035.7	1120	1094	1047

[a]Ref. [36]; [b]Ref. [5]; [c]Ref. [7]

3.4. Thermodynamic properties

Knowledge of the thermodynamic properties is essential to study the crystal stability and chemical reactivity, but reports about the thermodynamic properties of Sr-FAP have been very scarce so far. It is well known to us that the first-principles for phonon calculations are limited to $T = 0$ K yet the detailed thermodynamic properties of the crystals could be derived by phonons. In the present work, the phonon-related thermodynamic properties such as Helmholtz free energy F, internal energy E, entropy S, and specific heat at constant volume C_V are calculated using the formulas in Ref. [57] within the harmonic approximation. The predicted phonon-related thermodynamic properties under different temperature T for Sr-FAP and Ca-FAP are depicted in Fig. 6 and compared with the experimental values (Ca-FAP), in which the panels (a), (b), (c), and (d) are Helmholtz free energy F, internal energy of $E(T) - E(0)$, entropy S, as well as heat capacity at constant volume C_V, respectively. For studies at constant pressure, the appropriate thermodynamic function of enthalpy is $H = E + PV$. In our calculation, the equilibrium pressure equals zero, we consider the values of H are equal to E. So in Fig. 6(b) the experimental enthalpy values are chosen to compare with the internal energy E. The Helmholtz free energy F and internal energy E at zero-temperature can be calculated from the expression as follows:

$$F_0 = E_0 = 3nN \int_0^{\omega_{\max}} \frac{\hbar\omega}{2} g(\omega) \mathrm{d}\omega.$$

Where n is the number of atoms per unit cell, N is the number of unit cells, ω is the phonon frequencies, $g(\omega)$ is the normalized phonon density of states with $\int_0^{\omega_{\max}} g(\omega)\mathrm{d}\omega = 1$. In our calculation, $F_0 = E_0 = 293.4$ kJ/mol for Sr-FAP and 310.4 kJ/mol for Ca-FAP.

As shown in Fig. 6, the F decreases gradually with increasing temperature and the Ca-FAP has higher F than Sr-FAP, while $E(T) - E(0)$ increases almost linearly with increase in temperature and the differences for two apatites are quite small. We also note that the S increases with the applied temperature and the Sr-FAP has higher entropy than Ca-FAP, which can be explained by the larger contribution from the low phonon frequency for Sr-FAP. As for heat capacityC_V, we find both of them increase very rapidly in the low temperature (< 500 K). At high temperature, C_V tends to be a constant of 1034 J/K/mol that conforms to the well-known classical asymptotic limit of $C_V = 3nNk_B = 1047$ (J/K)/mol.

In comparison with the experimental results of Ca-FAP, we find that our calculated thermodynamic properties of Ca-FAP reveal good agreement with the experimental data. There are no experimental or theoretical works exploring the thermodynamic properties of crystal Sr-FAP to make a forceful comparison with the present data, which we hope can be a reference for the future study of the thermodynamic properties.

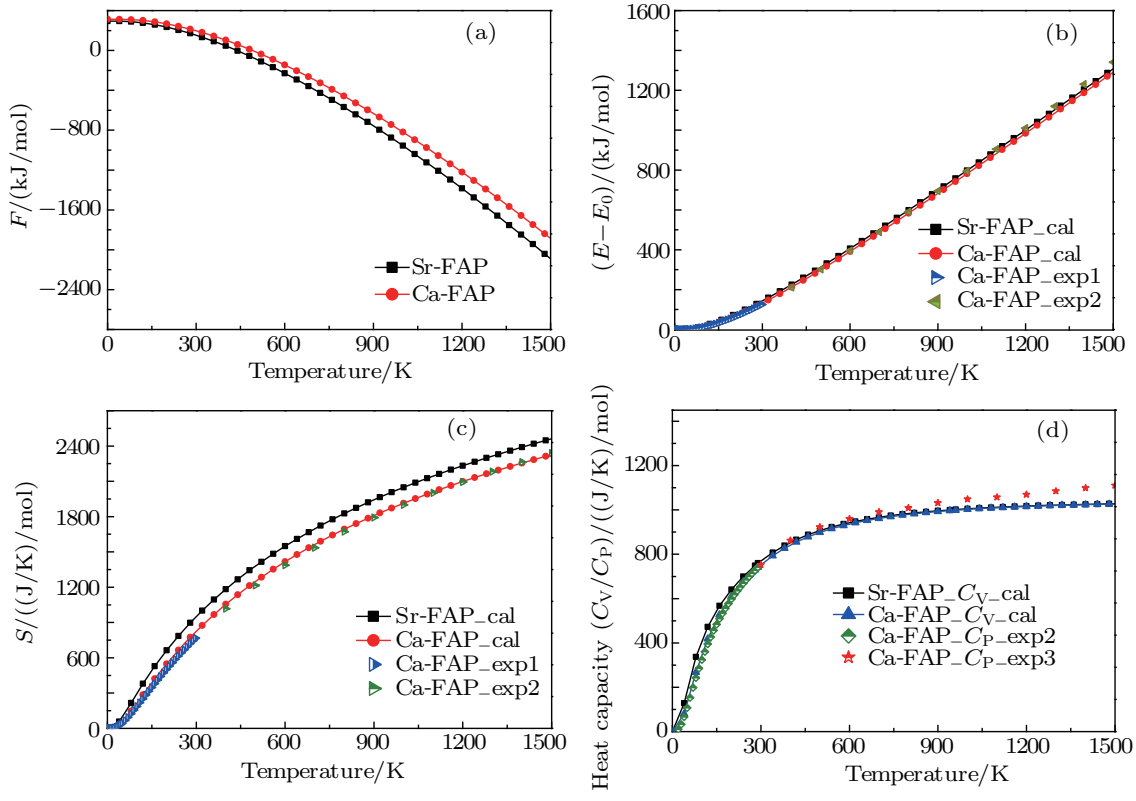


Fig. 6. (color online) The thermodynamic properties of Sr-FAP and Ca-FAP. (a) Helmholtz free energy F, (b) the internal energy E–E_0, (c) the entropy S, (d) the specific heat C_V exp1, exp2, and exp3 experimental data from Ref. [9], Ref. [11], and Ref. [14], respectively.

4. Conclusions

In summary, the electronic, elastic, vibrational, and thermodynamic properties of the crystal $Sr_{10}(PO_4)_6F_2$ and $Ca_{10}(PO_4)_6F_2$ have been systematically investigated using the first-principles calculations within GGA functions. With respect to two apatites, the relaxed lattice parameters are in good agreement with the experimental values, and the lattice parameters and cell volume of Sr-FAP are larger than Ca-FAP due to the ionic radius of Sr being higher than that of Ca. The calculated electronic properties indicate that the crystals Sr-FAP and Ca-FAP are insulator materials with the indirect band gap of 5.273 eV and 5.592 eV, respectively. The band gap decreases with substitutions of Ca by Sr. The calculated elastic constants of Sr-FAP and Ca-FAP are in reasonable agreement with the experiment and other theoretical data; the obtained elastic constants reveal the two apatites are mechanically stable. From elastic constants C_{ij}, the elastic modulus, such as bulk modulus, shear modulus, Young's modulus, and Poisson's ratio are further evaluated and discussed. The vibrational properties including the phonon dispersion curves, the phonon density of states, the Born effective charge, and associated LO–TO splittings of optical modes, as well as the phonon frequencies at zone-center are obtained within the DFPT. The Z^* diagonal components of Sr and F in Sr-FAP are larger than those of Ca and F in Ca-FAP, which means a stronger covalent characteristic for the Sr–F bond. The calculated vibrational frequencies agree well with the reported experimental infrared and Raman data. Additionally, as the atomic mass of the Sr atom is larger than that of the Ca atom, the Sr-FAP has lower phonon frequencies than those of Ca-FAP. Taking the long-range Coulomb (dipole–dipole) interaction into consideration, the associated LO–TO splitting is observed, and the modes A_u (2), A_u (6), E_{1u} (7), and E_{1u} (10) are barely affected by the long-range Coulomb interaction. Based on the calculated phonon density of states, the phonon-related thermodynamic properties such as the Helmholtz free energy F, the internal energy E, the entropy S, and the specific heat C_V are predicted and analyzed. We expect that our work will provide useful guidance for the better application of $Sr_{10}(PO_4)_6F_2$ in the future.

References

[1] Gross K A and Berndt C C 2002 *Reviews in Mineralogy and Geochemistry* **48** 631
[2] Kim H W, Lee S Y, Bae C J, Noh Y J, Kim H E, Kim H M and Ko J S 2003 *Biomaterials* **24** 3277
[3] Weber W J, Ewing R C, Catlow C, Rubia T D, Hobbs L, Kinoshita C, Matzke H, Motta A, Nastasi M and Salje E 1998 *J. Mater. Res.* **13** 1434
[4] Hendricks S, Jefferson M and Mosley V 1932 *Zeitschrift für Kristallographie-Crystalline Materials* **81** 352
[5] Adams D M, Gardner I R 1974 *J. Chem. Soc. Dalton Trans.* **14** 1505
[6] Majid C and Hussain M 1996 *Proceedings of the Pakistan Academy of Sciences* **33** 11
[7] Balan E, Delattre S, Roche D, Segalen L, Morin G, Guillaumet M, Blanchard M, Lazzeri M, Brouder C and Salje E K 2011 *Phys. Chem. Miner.* **38** 111
[8] Boyer L L and Fleury P A 1974 *Phys. Rev. B* **9** 2693
[9] Dachs E, Harlov D and Benisek A 2010 *Phys. Chem. Miner.* **37** 665
[10] Devarajan V and Klee W E 1981 *Phys. Chem. Miner.* **7** 35
[11] EganJr E P, Wakefield Z T and Elmore K L 1951 *J. Am. Chem. Soc.* **73** 5581
[12] Menéndez-Proupin E, Cervantes-Rodríguez S, Osorio-Pulgar R, Franco-Cisterna M, Camacho-Montes H and Fuentes M E 2011 *J. Mech. Behavior Biomed. Mater.* **4** 1011
[13] Rulis P, Ouyang L and Ching W Y 2004 *Phys. Rev. B* **70** 155104
[14] Fleche J L 2002 *Phys. Rev. B* **65** 245116
[15] Leroy N and Bres E 2001 *European Cells and Materials* **2** 36
[16] Chinthaka Silva G W, Hemmers O, Czerwinski K R and Lindle D W 2008 *Inorg. Chem.* **47** 7757
[17] Jay E E, Mallinson P M, Fong S K, Metcalfe B L and Grimes R W 2011 *J. Mater. Sci.* **46** 7459
[18] Rakovan J F and Hughes J M 2000 *The Canadian Mineralogist* **38** 839
[19] Li Z Y, Lam W M, Yang C, Xu B, Ni G X, Abbah S A, Cheung K M C, Luk K D K and Lu W W 2007 *Biomaterials* **28** 1452
[20] O'Donnell M, Fredholm Y, De Rouffignac A and Hill R 2008 *Acta Biomaterialia.* **4** 1455
[21] Shpak A, Karbovskii V and Kurgan N 2007 *J. Electron. Spectrosc. Relat. Phenom.* **156** 457
[22] Yuan X. Shen D Z, Wang X Q, Wang X Y, Wang R J and Shen G Q 2007 *Journal of Wuhan University of Technology-Mater. Sci. Ed.* **22** 205
[23] Pekov I V, Britvin S N, Zubkova N V, Pushcharovsky D Y, Pasero M and Merlino S 2010 *European Journal of Mineralogy* **22** 869
[24] Brenier A 2001 *J. Lumin.* **92** 199
[25] DeLoach L D, Payne S A, Smith L K, Kway W L and Krupke W F 1994 *J. Opt. Soc. Am. B* **11** 269
[26] Fang H S, Qiu S R, Zheng L L, Schaffers K I, Tassano J B, Caird J A and Zhang H 2008 *J. Crystal Growth* **310** 3825
[27] Qiao X B and Seo H J 2014 *J. Alloys Compd.* **615** 270
[28] Wang Q P, Zhao S Z, Zhang X Y, Sun L K and Zhang S J 1996 *Opt. Commun.* **128** 73
[29] Nagpure I M, Dhoble S J, Mohapatra M, Kumar V, Pitale S S, Ntwaeaborwa O M, Godbole S V and Swart H C 2011 *J. Alloys Compd.* **509** 2544
[30] Gloster L A W, Cormont P, Cox A M, King T and Chai B 1998 *Opt. Commun.* **146** 177
[31] Chai B Y, Hao L Y, Mao X J, Xu X, Li X K, Jiang B X and Zhang L 2016 *J. Am. Ceram. Soc.* **99** 1498
[32] Swafford S H, Holt E M 2002 *Solid State Sci.* **4** 807
[33] Schulte A, Buchter S C and Chai B H 1995 *Proc. SPIE* **34** 2380
[34] Bonner C E, Chess C C, Meegoda C, Stefanos S and Loutts G B 2004 *Opt. Mater.* **26** 17
[35] Zhai S M, Shieh S R, Xue W H and Xie T Q 2015 *Phys. Chem. Miner.* **42** 579
[36] Aissa A, Badraoui B, Thouvenot R and Debbabi M 2004 *Eur. J. Inorg. Chem.* **2004** 3828
[37] Chernorukov N, Knyazev A and Bulanov E 2011 *Inorg. Mater.* **47** 172
[38] Persson Kristin 2017 *Materials Project*, 1281477, 1280693
[39] Rabone J A L and De Leeuw N 2006 *J. Comput. Chem.* **27** 253
[40] Goryaeva A M, Urusov V S and Eremin N N 2013 *Eur. J. Mineral.* **25** 947
[41] Balachandran P V, Rajan K and Rondinelli J M 2014 *Acta Crystallographica Section B: Structural Science, Crystal Engineering and Materials* **70** 612
[42] Kresse G and Furthmüller J 1996 *Comput. Mater. Sci.* **6** 15
[43] Slepko A and Demkov A A 2011 *Phys. Rev. B* **84** 134108
[44] Yao H Z, Ouyang L Z and Ching W Y 2007 *J. Am. Ceram. Soc.* **90** 3194
[45] Perdew J P, Burke K and Ernzerhof M 1996 *Phys. Rev. Lett.* **77** 3865
[46] Monkhorst H J and Pack J D 1976 *Phys. Rev. B* **13** 5188
[47] Gonze X and Lee C 1997 *Phys. Rev. B* **55** 10355
[48] Wang Y, Shang S L, Fang H Z, Liu Z K and Chen L Q 2016 *npj Computat. Mater.* **2** 16006
[49] Baroni S, De Gironcoli S, Dal Corso A and Giannozzi P 2001 *Rev. Mod. Phys.* **73** 515
[50] Togo A and Tanaka I 2015 *Scripta Materialia* **108** 1-5
[51] Momma K and Izumi F 2011 *J. Appl. Crystallography* **44** 1272
[52] Li C X, Duan Y H and Hu W C 2015 *J. Alloys Compd.* **619** 66
[53] Sha M C, Li Z and Bradt R C 1994 *J. Appl. Phys.* **75** 7784
[54] Hill R 1952 *Proc. Phys. Soc. Section A* **65** 349
[55] Cang Y P, Lian S B, Yang H M and Chen D 2016 *Chin. Phys. Lett.* **33** 066301
[56] Haines J, Leger J and Bocquillon G 2001 *Ann. Rev. Mater. Res.* **31** 1
[57] Lee C and Gonze X 1995 *Phys. Rev. B* **51** 8610
[58] Boyer L L and Fleury P A 1974 *Phys. Rev. B* **9** 2693
[59] Devarajan V and Klee W E 1981 *Phys. Chem. Miner.* **7** 35
[60] Rulis P, Ouyang L and Ching W Y 2004 *Phys. Rev. B* **70** 155104